Received 1 July 2024; revised 23 July 2024; accepted 14 August 2024. Date of publication 26 August 2024; date of current version 22 November 2024.

Digital Object Identifier 10.1109/OJAP.2024.3449752

Beamforming Analysis of Dual Beam Antenna Array Using Theory of Characteristic Modes

MAHRUKH KHAN (Member, IEEE), TALHA MURAD (Student Member, IEEE), AND NICHOLAS LUSDYK

Electrical and Computer Engineering Department, The College of New Jersey, Ewing Township, NJ 08618, USA

CORRESPONDING AUTHOR: M. KHAN (e-mail: khanm@tcnj.edu)

This work was supported by the National Science Foundation under Grant 2138746.

ABSTRACT This paper presents a novel and insightful approach to beamforming a 2×2 antenna array using the theory of characteristic modes. The array comprises four rectangular patch antenna elements designed on an FR-4 substrate resonating at 2.4 GHz. The characteristic mode analysis (CMA) presented a fascinating physical insight into the surface current directions and the radiation characteristics of the array structure. The excitation of a specific characteristic mode led to the design of a dual-beam antenna array. After feed excitation, characteristic mode analysis (CMA) was employed to understand multi-beam pattern reconfigurability in the multi-port structure. The information of distinct and orthogonal modal characteristic fields guides the beamforming of multibeam arrays. Modal characteristic fields of specific modes were identified using a modal weighting coefficient that may combine upon port phase change for beamforming at a certain scan angle. The potential of multi-dimensional coverage of a multibeam array is presented by selecting the different phase combinations of feeding ports. The paper discusses the strengths and limitations of beam scanning due to the combination of modes. This physical insight is beneficial for future pattern reconfigurable antenna array design procedures. Measurements on a realized prototype are in a good agreement with simulations, proving the proposed concept.

INDEX TERMS Antenna arrays, beamforming, characteristic modes.

I. INTRODUCTION

RECONFIGURABLE antenna arrays have gained significant attention due to their adaptive ability in different complex scenarios by changing the frequency, pattern, and polarization [1], [2], [3], [4], [5], [6]. Among them, pattern reconfigurable antenna arrays are commonly known for increasing spectral efficiency and providing a more reliable radio communication link. These features make them desirable for emerging applications like radars and 5G/6G wireless communications. Moreover, It is relatively more straightforward to establish a steady data link and deal with environmental uncertainties and impairments by controlling the radiation pattern [7]. In addition, pattern reconfigurable antennas may minimize the interferences by positioning a null pattern in the direction of the unwanted signal or noise. Hence, they help improve the signal-to-interference ratio and the system performance [8]. The importance will further enhance if the array can point at multiple users simultaneously, i.e., multi/dual beam antenna array [9]. The multibeam reconfigurable antenna arrays will be of great importance for future applications where multidimensional coverage and fast communication rate will be required [10].

Characteristic mode analysis (CMA) has become a highly relevant and powerful analytical tool in the field of antenna design and analysis [11], [12], [13], [14], [15], [16], [17], [18], [19], [20], [21] due to its two main features. Firstly, the characteristic modes can give a physical insight into the resonant structure without excitation, which provides flexibility to choose optimal feed, leading to the systematic design of the antennas [14]. Secondly, the characteristic fields of the characteristic modes are orthogonal, providing great help for designing MIMO antennas [16], pattern reconfigurable antennas [17], and super directive antennas [19]. In [15], it was shown how the information of multiple significant modes helps to improve the envelope correlation coefficient for the MIMO antenna. In addition, knowledge of the coupling between excitation and significant modes enables a designer to synthesize the desired antenna pattern [25].

Reactive loading is successfully applied in [23] to control the radiation pattern mounted on the platform radiator. In [26], a systematic method for pattern synthesis is presented where a desired pattern was obtained based on the maximum correlation between modes and the desired pattern. The fact that the phases of the feedings can control the excitation or suppression of the modes helped in a desired up-tilted pattern beam for the RFID (Radio Frequency IDentification) antenna in [27]. The drawback is that only the maximum radiation is ensured without considering the patterns in other directions.

Similarly, the null of the antenna pattern can be steered by shifting the relative phases of different modes using capacitive exciters [8]. Most pattern synthesis methods in literature depend on the optimization process to explore the desired combination of modes [26]. Instead, it was shown in [18] that the inherent pattern and phase properties within different modes can offer a better understanding of the radiation mechanism. In addition, characteristic modes with distinctive radiation patterns and phase characteristics within a frequency band can be combined in pairs to generate frequency scanning beams [5]. An interesting beamforming concept for the multibeam antenna is presented in [28], showing how orthogonal modal radiation patterns can be combined for beamforming at the desired scan angle. However, the antenna design still needs to be discussed in detail.

This paper presents a detailed beamforming analysis of a dual beam antenna array using characteristic modes by changing the feeding phases. It has shown how modal electric fields helped in the intuitive beamforming of dual beam arrays. This simple, low-cost dual-beam antenna array was designed and fabricated using characteristic modes. The information on natural characteristic modes and significant modes from the modal weighting coefficient helped identify the modal radiation patterns that may participate in the beamforming. Three cases have been discussed to describe the potential multidimensional coverage of multibeam arrays. In each case, the phase change of the feeding ports was used to select two significant modes combined to generate a beam at a particular angle. The paper discussed the array's coverage in azimuth and elevation plane and its limitations in each plane.

II. STRUCTURE OF THE ANTENNA ARRAY

The array's configuration under analysis is shown in Fig. 1. The array consists of four identical elements of rectangular microstrip patches in a 2×2 rectangular lattice. The flat metal pieces of the array elements are simulated as perfect electric conductor (PEC) above an infinite ground plane and etched on top of a printed circuit board with an FR-4 substrate(lossless) ($\epsilon_r = 4.3$) and with a thickness of 1.6 mm. The spacing between array elements is 0.45λ(λ is the wavelength at 2.4 GHz). The unit cell's length(L) and width(W) are 29.37 mm and 38.27 mm, respectively.

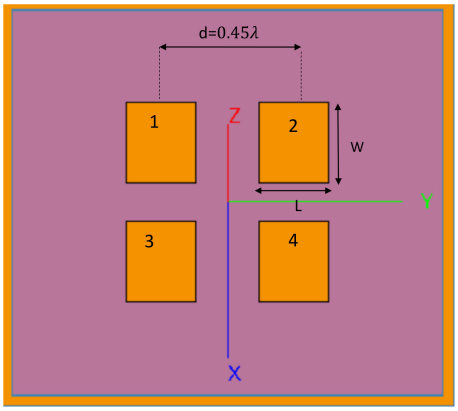

FIGURE 1. Configuration of a 2 × 2 array before feed excitation.

III. CHARACTERISTIC MODE ANALYSIS OF THE ANTENNA ARRAY

In this paper, we used Altair FEKO 2021/2022 for simulations. The CMs analysis allows obtaining a set of orthogonal current modes (Jn) distribution that depends only on the antenna geometry and is independent of any external excitation [13]. Once these current modes (J_n) are known, the total current distribution (J_{tot}) over the investigated structure can be decomposed as a liner superposition of these modes

$$J_{tot} = \sum_{n=1}^{N} \alpha_n J_n(\theta, \phi) \tag{1}$$

where α_n is the complex MWC (modal weighting coefficient) of the n^{th} mode excited by the antenna array. The far-field pattern of the antenna array can be expressed as a linear superposition of the characteristic fields:

$$F(\theta, \phi) = \sum_{n=1}^{N} \alpha_n E_n(\theta, \phi) \tag{2}$$

where α_n is the complex MWC of the n^{th} mode, and E_n is the corresponding electric field. Intuitively, α_n stands for the contribution of each mode to the total radiation pattern.

A. CHARACTERISTIC MODES BEFORE FEED EXCITATION

The characteristic mode analysis(CMA) of the 2 × 2 array was performed. The 2 × 2 array was simulated without feed. The antenna array's modal significance(MS) is shown in Fig. 4(a), which shows eight natural characteristic modes of the structure. The first four modes are excited at 1.86 GHz, and the last four reached their peak at 2.4 GHz. The array's surface currents and electric field at their peak frequencies are shown in Figs. 2 and 3. The total surface current can be expressed as:

$$\begin{aligned} J_{tot} = {} & \alpha_1 J_1 + \alpha_2 J_2 + \alpha_3 J_3 + \alpha_4 J_4 \\ & + \alpha_5 J_5 + \alpha_6 J_6 + \alpha_7 J_7 + \alpha_8 J_8 \end{aligned} \tag{3}$$

where MS>0.707 at 1.86 GHz for J_1, J_2, J_3 and J_4 and MS>0.707 at 2.4 GHz for J_5, J_6, J_7 and J_8.

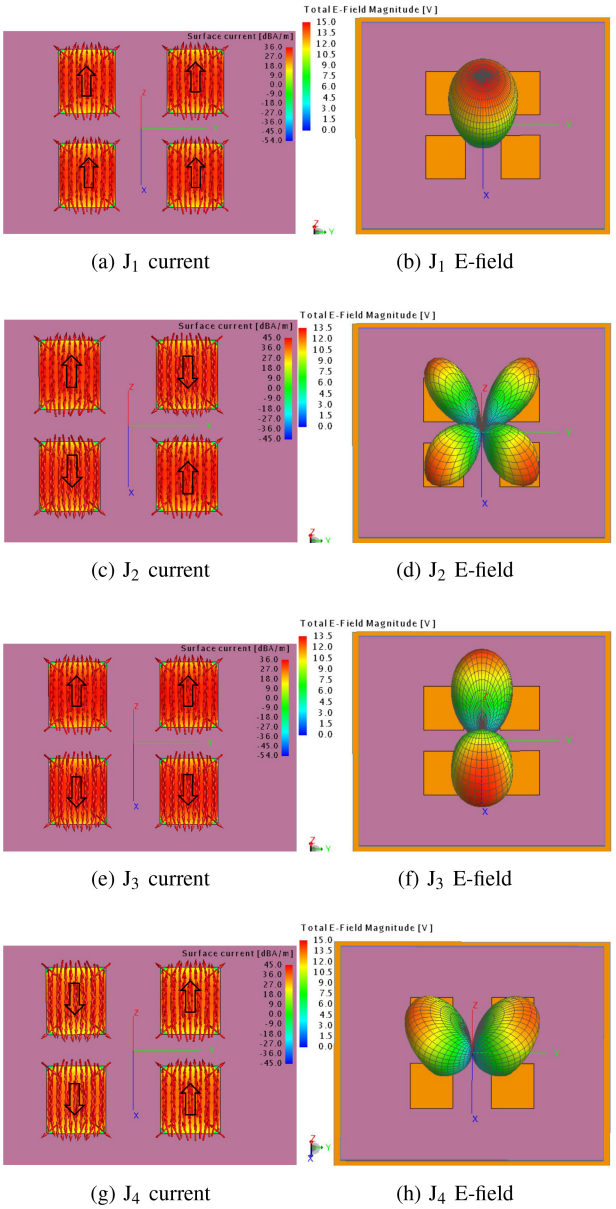

(a) J_1 current (b) J_1 E-field

(c) J_2 current (d) J_2 E-field

(e) J_3 current (f) J_3 E-field

(g) J_4 current (h) J_4 E-field

FIGURE 2. Surface currents(J_n) and CM fields of natural CMs at 1.86 GHz.

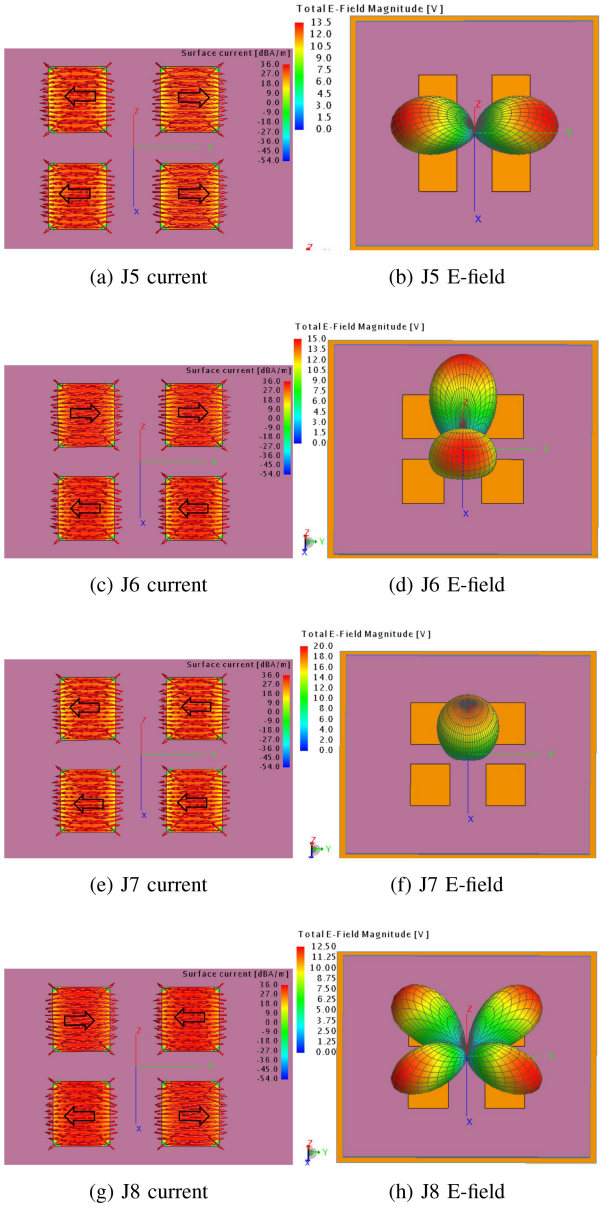

(a) J5 current (b) J5 E-field

(c) J6 current (d) J6 E-field

(e) J7 current (f) J7 E-field

(g) J8 current (h) J8 E-field

FIGURE 3. Surface currents(J_n) and CM fields of natural CMs at the resonant frequency.

Four types of radiation patterns can be seen. The first type is the one main directional lobe for J_1 and J_7. One main lobe occurs when all patches have surface currents in the same direction (See Fig. 2(a) and (b) and Fig. 3(e) and (f)). The current direction is vertical for J_1 and horizontal for J_7. The second type of dual lobe pattern occurs when two of the four elements have the same current direction. In Fig. 2(f) and Fig. 3 (d), it can be seen for J_3 and J_6 that two lobes occurred in the direction of the x-axis when elements 1 and 2 have the same direction of current and element 3 and 4 have the same direction but opposite to the direction of 1 and 2. The difference between J_3 and J_6's current modes is that J_3's current is in vertical or x-axis direction, and mode 6's are in horizontal direction. The 3rd type of radiation pattern is when two opposite lobes are produced in the y-axis direction for J_4 and J_5 (See Fig. 2(h) and Fig. 3 (b)). This phenomenon occurs when elements on the side of the lobe have a current in the same direction, such as elements 1 and 3 showing a current in the same direction and elements 2 and 4 showing a current in the same direction. J_4 exhibited currents in the vertical direction, while J_5 exhibited currents in the horizontal direction. The fourth type of pattern occurred when all patches showed current in different directions from each other, resulting in four lobe radiation patterns. J_2 and J_8 showed this behavior in Fig. 2(d) and Fig. 3(h). It can be observed that currents in J_2 are vertical, and in J_8 are horizontal. It can be concluded that eight modes exhibited four types of radiation patterns with vertical and horizontal currents. That means the array can produce four types of radiation patterns upon proper excitation.

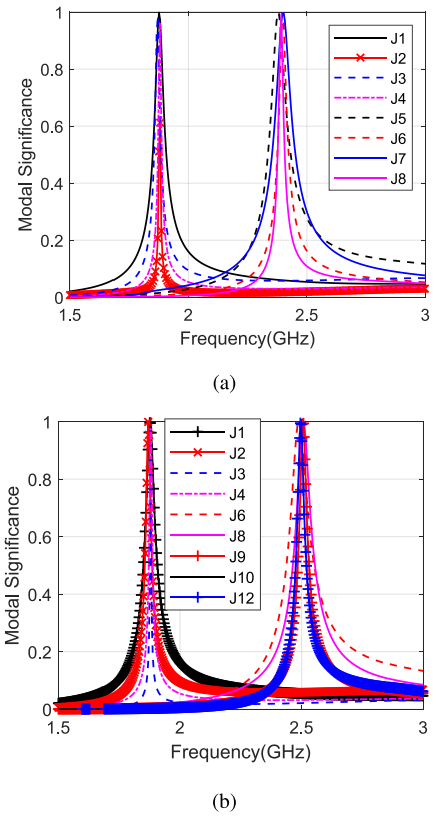

FIGURE 4. Modal Significance of the antenna array (a) before excitation (natural characteristic modes) (b) after excitation.

Considering the array is mounted on an infinite ground plane, based on the cavity model [9], the radiation of the antenna array of each current mode can be modeled as

$$E_{J_1} = E_{J_7} = \begin{bmatrix} e^{\frac{jkd_x sin\theta cos\phi}{2}} & e^{\frac{-jkd_x sin\theta cos\phi}{2}} \\ e^{\frac{jkd_y sin\theta sin\phi}{2}} & e^{\frac{-jkd_y sin\theta sin\phi}{2}} \end{bmatrix} \times \begin{bmatrix} 1 & 1 \\ 1 & 1 \end{bmatrix} \tag{4}$$

$$E_{J_3} = E_{J_6} = \begin{bmatrix} e^{\frac{jkd_x sin\theta cos\phi}{2}} & e^{\frac{-jkd_x sin\theta cos\phi}{2}} \\ e^{\frac{jkd_y sin\theta sin\phi}{2}} & e^{\frac{-jkd_y sin\theta sin\phi}{2}} \end{bmatrix} \times \begin{bmatrix} 1 & 0 \\ -1 & 0 \end{bmatrix} \tag{5}$$

$$E_{J_4} = E_{J_5} = \begin{bmatrix} e^{\frac{jkd_x sin\theta cos\phi}{2}} & e^{\frac{-jkd_x sin\theta cos\phi}{2}} \\ e^{\frac{jkd_y sin\theta sin\phi}{2}} & e^{\frac{-jkd_y sin\theta sin\phi}{2}} \end{bmatrix} \times \begin{bmatrix} 0 & 1 \\ 0 & -1 \end{bmatrix} \tag{6}$$

$$E_{J_2} = E_{J_8} = \begin{bmatrix} e^{\frac{jkd_x sin\theta cos\phi}{2}} & e^{\frac{-jkd_x sin\theta cos\phi}{2}} \\ e^{\frac{jkd_y sin\theta sin\phi}{2}} & e^{\frac{-jkd_y sin\theta sin\phi}{2}} \end{bmatrix} \times \begin{bmatrix} 1 & 1 \\ -1 & -1 \end{bmatrix} \tag{7}$$

where $k = \frac{2\pi}{\lambda}$, θ and ϕ determine the radiation angle in the 2D plane, d_x is the distance between elements in the x-axis direction and d_y is the y-axis direction. Intuitively, it can be seen from the above equations that

1) The first type is the usual type of excitation when all feeds are in the same direction and the radiation lobe is pointing towards θ=0°.
2) J_3 and J_6 lobes can be excited when the phase shift between element 1 and element 3 is 180° and element 1, and element 2 are zero, which causes a dual beam in the x-axis direction.
3) J_4 and J_5 can be excited when the phase shift between elements 1 and 3 is zero, and the phase shift between elements 1 and 2 is 180°.
4) J_2 and J_8 can be excited when all feeds are opposite each other, exciting different currents for each patch.

TABLE 1. Modal behavior of current modes and radiation patterns before feed excitation.

Modes	Radiation Pattern Types	Current direction(axis)of elements {1,2,3,4}
J_1	One lobe directed to $\theta = 0^o$	{x,x,x,x}
J_2	Four lobe perpendicular to each other	{x,-x,-x,x}
J_3	Two lobes in x-axis	{x,x,-x,-x}
J_4	Two lobes in y-axis	{-x,x,-x,x}
J_5	Two lobes in y-axis	{-y,y,-y,y}
J_6	Two lobes in x-axis	{y,y,-y,-y}
J_7	One lobe directed to $\theta = 0^o$	{-y,-y,-y,-y}
J_8	Four lobe perpendicular to each other	{y,-y,-y,y}

Table 3 summarizes the whole scenario. The dual beam, which is the outcome of excitation of J_3, J_4, J_5, and J_6, can produce a greater number of beams than a single beam array. In the next section, a dual beam antenna array was designed by exciting a mode (J_5) with a dual beam in the direction of the y-axis.

IV. DUAL BEAM ANTENNA ARRAY

After excitation, the effect of antenna feed can be shown through input admittance at the feed point (P).

$$Y_{in}[P] = \sum Y_n = \sum_n \frac{V_n^i J_n(P)}{1 + \lambda_n^2}(1 - j\lambda_n) \tag{8}$$

where Y_n is the modal admittance. The subscript (P) denotes the current sampling point at the antenna port, and α can be expressed as

$$\alpha_n = \frac{V_n^i}{1 + j\lambda_n} \tag{9}$$

Hence, Y_n will become

$$Y_{in} = \sum_n \alpha_n J_n(P) \tag{10}$$

which shows the dependence of input admittance on the feed excitation and modal weighting coefficient. In the above

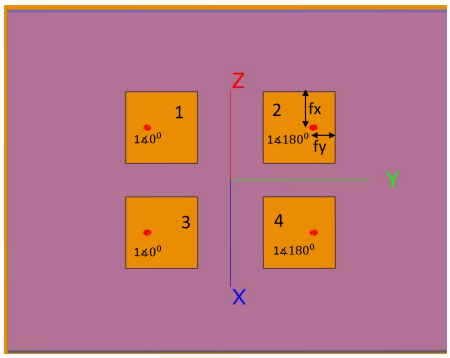

FIGURE 5. Configuration of the array after feed excitation.

structure, it can be observed that the natural mode with a dual beam in the y direction, i.e., J_5, can be excited by placing the feeds in the direction of currents. Hence, the feed position for elements 1 and 3 is opposite to elements 2 and 4. The opposite feed position will put elements 2 and 4 at the 180° phase with elements 1 and 3 as shown in Fig. 5. The simple probe feeding technique will allow the desired feeding network to be added for the beam scanning in theta and phi directions. The array factor of a 2×2 planar array can be written as

$$AF = e^{jkd_x sin(\theta_0)cos(\phi_0)+\beta_x} + e^{jkd_y sin(\theta_0)sin(\phi_0)+\beta_y} \quad (11)$$

where progressive phase shift of 2D planar array β_x and β_y can be calculated as given

$$\beta_x = -kd_x sin\theta_0 cos\phi_0 \quad (12)$$

$$\beta_y = -kd_y sin\theta_0 sin\phi_0 \quad (13)$$

where $d_x = d_y = 0.45\lambda$. For the current case, i.e., $\beta_y = 180°$ $\beta_x = 0°$, the dual-beam was produced as shown in Fig. 10 at a scan angle $\theta_o = +/-55$ degrees and $\phi_o = 90$ degrees. The dual beam's beamwidth is 61°, showing a peak gain 8 dBi. The antenna array showed stable gain with a cross-polarization level as low as −60 dB.

After feed excitation, The total surface current can be expressed as

$$J_{tot} = \alpha_1 J_1 + \alpha_2 J_2 + \alpha_3 J_3 + \alpha_4 J_4 + \alpha_6 J_6 + \alpha_8 J_8 + \alpha_9 J_9 + \alpha_{12} J_{12} \quad (14)$$

Subsequently, the far field produced can be expanded using related characteristic mode fields by

$$\sum E_n \alpha_n \approx \alpha_1 E_1 + \alpha_2 E_2 + \alpha_3 E_3 + \alpha_4 E_4 + \alpha_6 E_6 + \alpha_8 E_8 + \alpha_9 E_9 + \alpha_{12} E_{12} \quad (15)$$

However, it has been observed that significant modes that have shown MS>0.707 at resonant frequency are J_6, J_8, J_9, and J_{12} (see Fig. 4(b)). After excitation, the J_5 natural mode corresponds to J_6, J_6 (natural) corresponds to J_8, J_7 (natural) corresponds to J_9, and J_8 (natural) corresponds to J_{12}. These four modes show a similar pattern for the direction of currents as their corresponding natural modes, and all

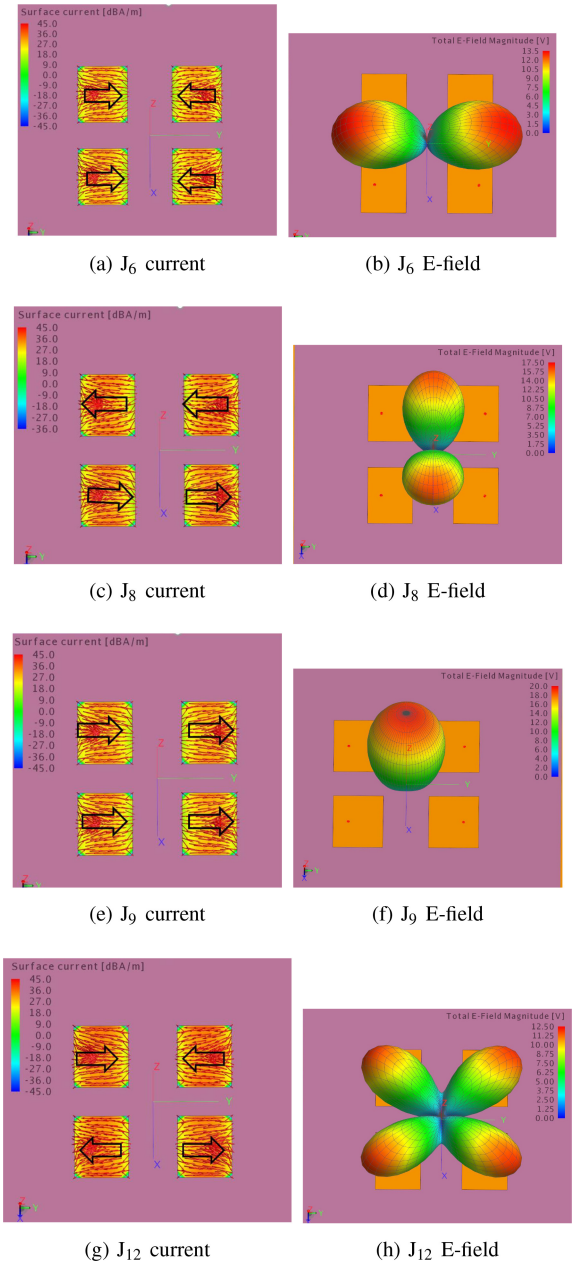

(a) J_6 current (b) J_6 E-field

(c) J_8 current (d) J_8 E-field

(e) J_9 current (f) J_9 E-field

(g) J_{12} current (h) J_{12} E-field

FIGURE 6. Surface currents and CM fields of the array after excitation at the resonant frequency.

four types of radiation patterns are shown in Fig. 6. After excitation, a slight shift in resonant frequency was observed for characteristic modes, as the maximum modal significance was at approximately 2.5 GHz.

A comprehensive characteristic mode analysis was performed by changing the phase of the ports in simulations. It has also been observed that multiple modes contribute as a phase of the input ports has been changed. The modal behavior was explained using the modal weighting coefficient, surface currents, and electric fields. Based on the scan angle, three cases of beamforming were discussed as follows:

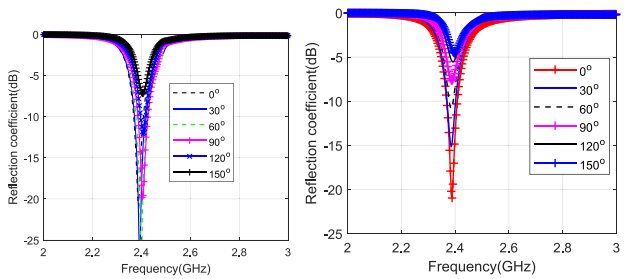

(a) Port 1 (b) Port 2

FIGURE 7. Reflection coefficient of multiports of the array for Case I.

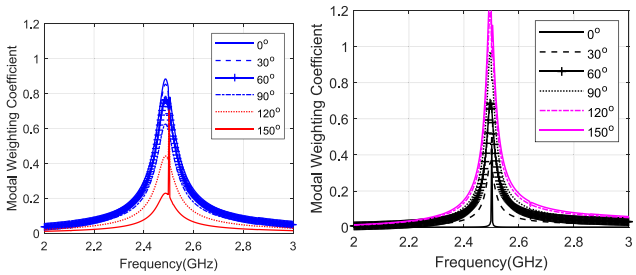

(a) J_6 (b) J_{12}

FIGURE 8. Modal weighting coefficient of the dual beam array (Case I).

A. CASE I

In the first case, the initial phase of elements 1 and 2 is 0 degrees, producing a dual beam at an angle of $\theta = +/-55°$ and $\phi = 90°$. The overall phase of the ports is shown in Fig. 9, and the phase of both elements incremented by 30 degrees. The phase change excited the J_{12}, contributing to the overall radiation pattern and altering the scan angle of the dual beam in phi direction for 6 degrees approx for every 30-degree increments (See Fig. 10). Fig. 10(b) showed the deterioration in the cross-polarization with phase change. The cross-pol was less than -10 dB till the input phase was 60 degrees. It can be observed that The contribution of J6 and J12 with phase change can be seen from the modal weighting coefficient plot in Fig. 8. The total far-field produced can be expressed as

$$\sum E_n \alpha_n \approx \alpha_6 E_6 + \alpha_{12} E_{12} \tag{16}$$

As the ports 1 and 2's phase increases, the antenna's radiation pattern becomes a combination of J_{12} and J_6 such that J_{12} becomes the dominant mode and J_6 loses its significance. However, the reflection coefficient for all ports showed deterioration in the impedance matching. The reflection coefficient of ports 1 and 2 is less than -10 dB till the phase of the ports was 60°, as shown in Fig. 7. The gain remains stable at 8 dBi for all scan angles. Similar results were obtained when the phase of elements 3 and 4 was incremented by 30 degrees, except the scan angle changed in the opposite direction. Case I outputs are summarized in Table 2.

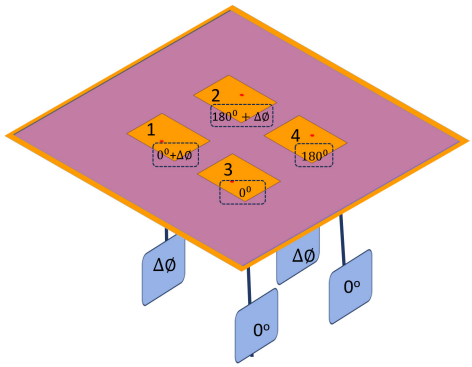

FIGURE 9. Overall initial phase of the ports for Case I.

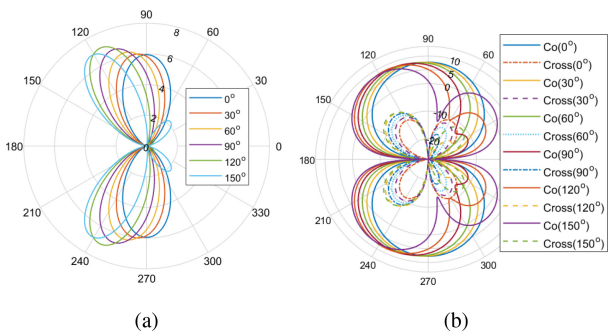

(a) (b)

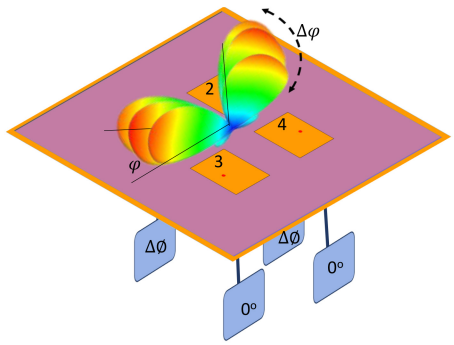

(c)

FIGURE 10. Radiation pattern and beam steering of the antenna array for Case I (a) Linear polar plot @($\theta = 55°$) (b) Co-pol and cross-pol components in dB@ ($\theta = 55°$) (c) 3D radiation pattern.

TABLE 2. Beam position with port phase change for Case I.

Phase Ports{1,3}	Phase Ports{2,4}	Radiation Pattern (θ,ϕ) (degrees)	Gain(dBi)
{0^o,0^o}	{0^o,0^o}	Dual beam(55^o,90^o)	8dBi
{30^o,0^o}	{30^o,0^o}	Dual beam(55^o,96^o)	8dBi
{60^o,0^o}	{60^o,0^o}	Dual beam(55^o,103^o)	8dBi
{90^o,0^o}	{90^o,0^o}	Dual beam(55^o,110^o)	8dBi
{120^o,0^o}	{120^o,0^o}	Dual beam(55^o,116^o)	8.4dBi
{150^o,0^o}	{150^o,0^o}	Dual beam(55^o,122^o)	8.2dBi

B. CASE II

In the second case, the phase of elements 1 and 2 was adjusted to be 180 degrees to keep the overall phase of all elements at 0 degrees (shown in Fig. 13) that excite J_9's

TABLE 3. Beam position with port phase change for Case II.

Phase Ports {1,3}	Phase Ports {2,4}	Radiation Pattern(θ, ϕ)	Gain(dBi)
$\{0^o,0^o\}$	$\{180^o,180^o\}$	Single lobe directed to$(0^o,0^o)$	10.5
$\{30^o,0^o\}$	$\{210^o,180^o\}$	$(-7^o,0^o)$	10.5
$\{60^o,0^o\}$	$\{240^o,180^o\}$	$(-13^o,0^o)$	10.6
$\{90^o,0^o\}$	$\{270^o,180^o\}$	$(-19^o,0^o)$	10.6
$\{120^o,0^o\}$	$\{300^o,180^o\}$	$(-26^o,0^o)$	10.58
$\{150^o,0^o\}$	$\{330^o,180^o\}$	$(-32^o,0^o)$	10.036

TABLE 4. Beam position with port phase change for Case III.

Phase(Ports 1,3)	Phase(Ports 2, 4)	Radiation Pattern(θ, ϕ)	Gain(dBi)
$90^o,-90^o$	$-90^o,90^o$	Dual beam$(38^o,360^o)$	8.7
$90^o+30^o,-90^o$	$-90^o+30^o,90^o$	Dual beam$(39^o,347^o)$	8.7
$90^o+60^o,-90^o$	$-90^o+60^o,90^o$	Dual beam$(42^o,335^o)$	8.7
$90^o+90^o,-90^o$	$-90^o+90^o,90^o$	Dual beam$(46^o,326^o)$	8.7
$90^o+120^o,-90^o$	$-90^o+120^o,90^o$	Dual beam$(52^o,318^o)$	8.5
$90^o+150^o,-90^o$	$-90^o+150^o,90^o$	Dual beam$(58^o,318^o)$	8.45

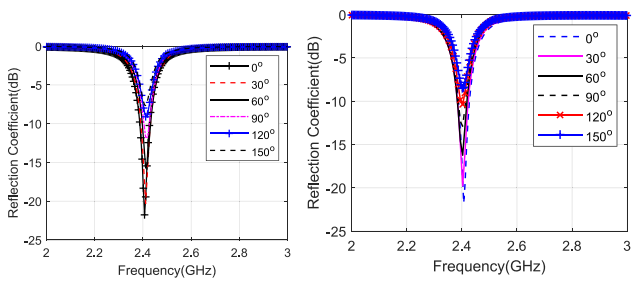

(a) Port1 (b) Port3

FIGURE 11. Reflection coefficient of multiports of the array for Case II.

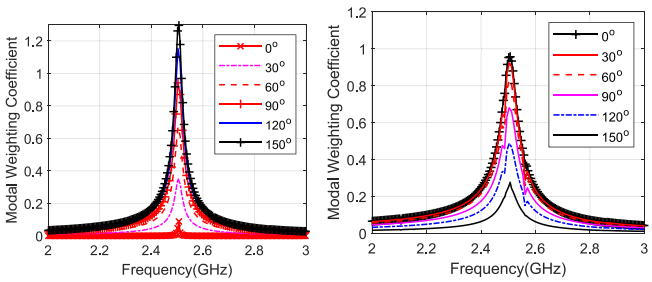

(a) J8 (b) J9

FIGURE 12. Modal weighting coefficients of the antenna array for Case II.

single lobe pointing towards $\theta = 0°$. To steer the beam in the $-$x direction, the phases of element one and element two were incremented by 30 degrees, which excited J_8. To

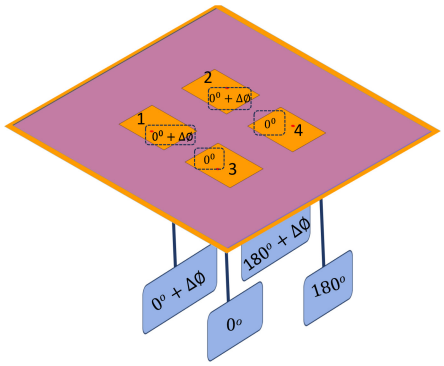

FIGURE 13. Overall phase of the ports for Case II.

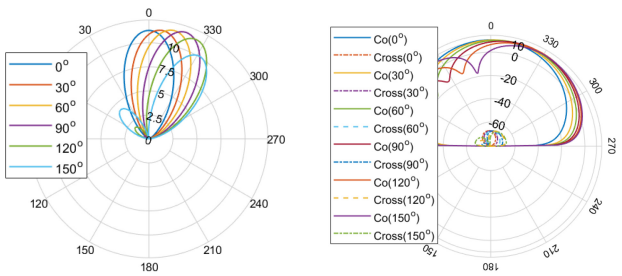

(a) (b)

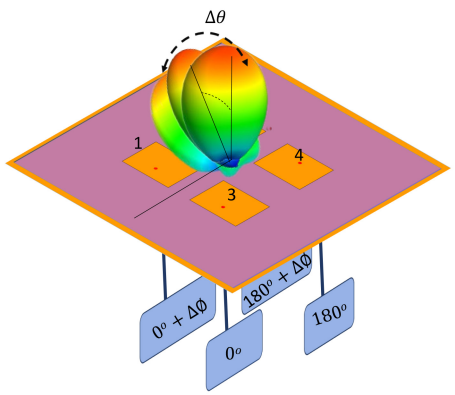

(c)

FIGURE 14. Radiation pattern and beam steering of the antenna array for Case II (a) Linear polar plot @($\phi = 0°$) (b) Co-pol and cross-pol components in dB@($\phi = 0°$) (c) 3D radiation pattern.

scan the beam angle in the other direction, elements 3 and 4 phases must be adjusted. The presence of J_8 helped to steer the beam in $+$x and $-$x directions. The far-field produced can be expanded using related characteristic mode fields by

$$\sum E_n \alpha_n \approx \alpha_8 E_8 + \alpha_9 E_9 \tag{17}$$

The contribution of J_8 and J_9 is also shown in Fig. 12. It can be seen that mode 9 is dominant for 0 degrees, but J_8 becomes dominant as the port phase changes. The overall gain is 10 dBi for all angles, more than Case I (See Fig. 14). It can also be seen from Fig. 14(b) that cross-polarization is less than -60 dB for all phase changes,

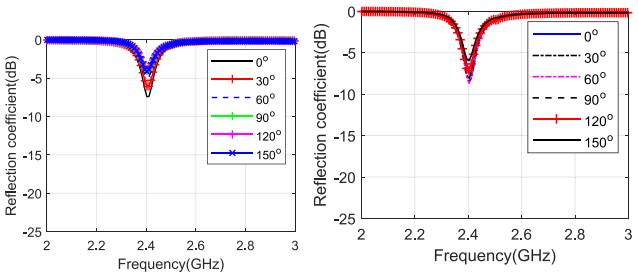

(a) Port1 (b) Port2

FIGURE 15. Reflection coefficient of the antenna array for Case III.

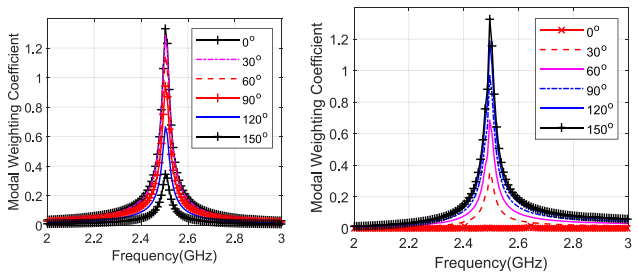

(a) J8 (b) J12

FIGURE 16. Modal weighting coefficient of the antenna array for Case III.

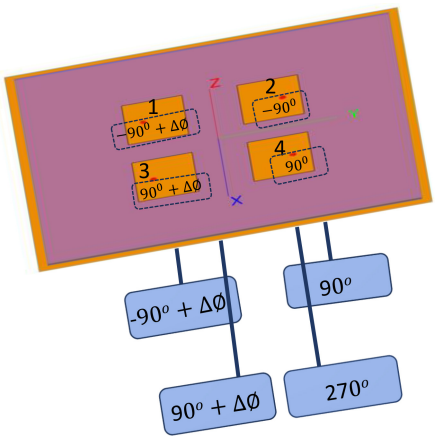

FIGURE 17. Overall phase of the ports for Case III.

showing good cross-polarization discrimination(XPD) at the resonant frequency. The reflection coefficient of port1 and port2 showed more deterioration than port3 and port4 (See Fig. 11). The reflection coefficient of ports 1 and 2 is less than −10dB till the phase of the ports was 120°. Similar results were obtained when the phase of elements 3 and 4 was incremented by 30 degrees, except the scan angle changed in the opposite direction. Case II outputs are summarized in Table 2.

C. CASE III

In the third case, the phase of elements 1 and 3 was adjusted to be 90 degrees, and elements 2 and 4 were adjusted to be −90 degrees (See Fig. 17). The idea was to try to steer the beam in theta direction by exciting J_8 mode. It can seen from

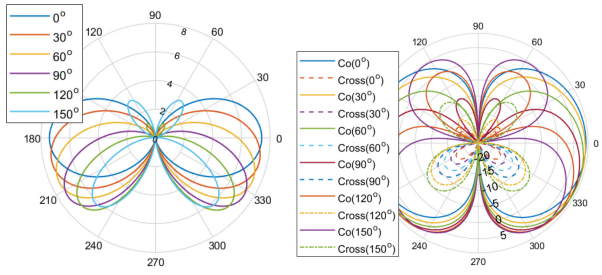

(a) (b)

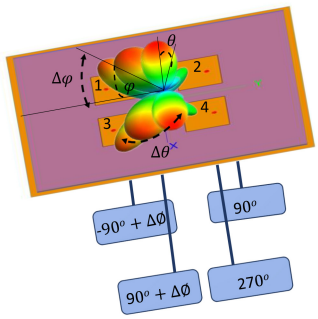

(c)

FIGURE 18. Radiation pattern and beam steering of the antenna array for Case III (a) Linear polar plot (b) Co-pol and cross-pol components in dB (c) 3D radiation pattern.

the modal weighting coefficient plot in Fig. 16 that J8 was excited initially, then J12 participated and became dominant as the phase was incremented by 30 degrees. The far-field produced can be expanded using related characteristic mode fields by

$$\sum E_n \alpha_n \approx \alpha_8 E_8 + \alpha_{12} E_{12} \tag{18}$$

The beam steered in both theta and phi direction as shown in Fig. 18. It was also observed in Fig. 15 that impedance matching was poor, i.e., −8 dB for that case, owing to the rectangular shape of the element. The overall gain is 8.7 dBi for all angles. The antenna array's cross-pol is more sensitive to phase change in this case than in the other two cases, as shown in Fig. 18(b). With phase change, cross-polarization discrimination varied from 30 dB to 10 dB. A step-by-step design procedure is summarized in Fig. 19. It can also be concluded from characteristic mode analysis that the dual beam can be steered in both azimuth and elevation planes using phase change in the feed port. Still, it certainly has limitations over steering due to deterioration in impedance matching. Here are a few takeaways from the design and analysis.

1) The array structure is simple. The array is low-cost. It is easy to adapt a simple feeding structure.
2) The dual beam antenna array offers enhanced coverage in both directions
3) The dual beam array steering capability in all directions can be further improved by improving its mutual coupling.

TABLE 5. Comparison of Beamforming Techniques.

Beamforming Type	Methodology	Features
Hybrid Beamforming [29]	A technique that suppresses the spatial interference that enhances the signal-to-interference-plus-noise ratio (SINR) by forming an interference-canceling beam. A deep spatial notch was created by spatially combining the array factors (AFs) of the main beam and the interference-canceling beam without main beam power degradation.	+ software based +handle large antenna arrays + number of beams can be changed dynamically with no change in hardware. - Computationally extensive - Costly
Adaptive Beamforming [30]	The proposed scheme consists of a DNN(deep neural network) based beamformer and a subspace tracking-based multiple signal classification (MUSIC) estimator. Specifically, the DNN generates the beamformer using soft AoA(angle of Arrival) estimates from the previous time block, and the MUSIC estimator exploits the measured signal to estimate the AoAs in the current time block.	+ suitable for dynamic beam applications such as UAVs, etc. +change directional sensitivity without physically moving an array of receivers -computationally extensive - Expensive
Switched Beamforming[[1]	Generate ten (10) switched-beams in 2-D space when series fed elements are excited from respective ports through 3 dB quadrature couplers	+hardware based + low cost + less computationally extensive - fixed number of beams
Beamforming Using Characteristic Modes[This paper]	The information of distinct and orthogonal modal characteristic fields guides the beamforming of multibeam arrays. Modal characteristic fields of specific modes were identified using a modal weighting coefficient that may combine upon port phase change for beamforming at a certain scan angle. The potential of multi-dimensional coverage of a multibeam array is presented by selecting the different phase combinations of feeding ports.	+ less computationally extensive + low cost + potential for multidimensional coverage with a simpler array - fixed number of beams

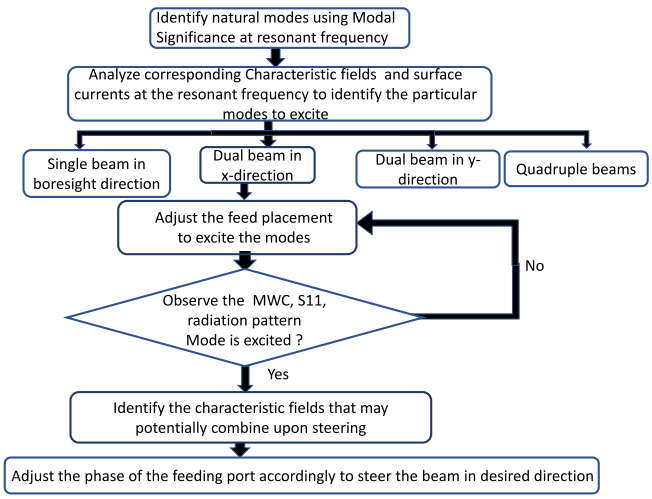

FIGURE 19. A systematic procedure of the array beamforming using characteristic modes.

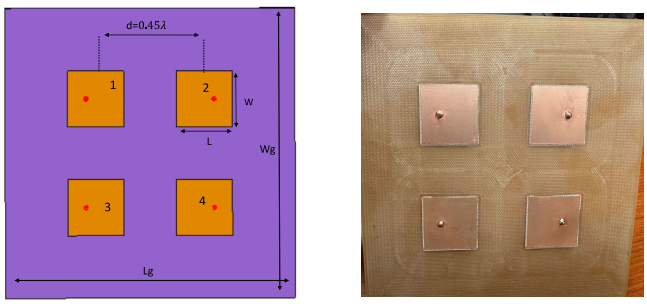

(a) Simulated (b) Fabricated

FIGURE 20. Optimized Design of the antenna array (Dimensions: $\epsilon_r = 4.3$, $tan(\delta) = 0.03$, L = W = 27.5mm, Lg = Wg = 75mm).

4) Its ability to generate the beams in different directions makes it a suitable candidate for adapting diverse application scenarios.
5) The steering can be predicted and controlled by analyzing the radiation patterns of natural characteristic modes.

V. MEASUREMENT RESULTS

The characteristic mode analysis of the 2 × 2 array was performed using an infinite ground plane. After beamforming analysis, the antenna array was designed on the finite ground plane. The losses due to the finite ground plane deteriorated the reflection coefficient, and the antenna array needed some optimization. After optimization, the antenna array was fabricated in TCNJ's Microwave and Wireless Communication lab using LPKF S104, as shown in Fig. 20. The measured and simulated antenna reflection coefficients are shown in Fig. 21(a). The measured and simulated mutual coupling is also shown in Fig. 21(b). Overall, there is a reasonable agreement between measured and simulated results. However, a slight shift was observed in mutual coupling plots, possibly due to human error during in-house fabrication and experimental imperfections. It can be observed that the mutual coupling between elements 1 and 3 is poorer than it is between other elements.

The radiation pattern measurements were also performed at 2.5 GHz in the Star Lab 18 GHz measurement system in TCNJ (The College of New Jersey). The measured radiation

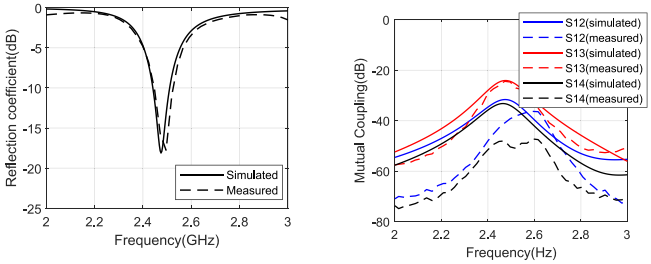

(a) Reflection Coefficient (b) Mutual Coupling

FIGURE 21. Simulated vs measured results of the antenna array.

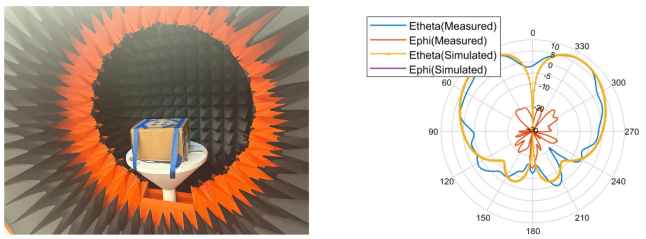

(a) Pattern measurement in Star-Lab (b) Radiation Pattern @2.5 GHz

FIGURE 22. Simulated vs measured results of the antenna array.

pattern agreed well with the simulated results, as shown in Fig. 22. The radiation pattern showed dual beam behavior for $\phi = 90°$, but higher cross-pol was observed, which can be expected in the practical measurements. The measurements proved that a particular current mode can be effectively excited to produce multibeam behavior in the simple antenna array. The feed network for phase change will be added in future work. Table V compares this beamforming technique with current methods. The table compares the methodology and features of all techniques.

VI. CONCLUSION

A beamforming analysis of a simple dual-beam antenna array was presented. The basic idea is to manipulate the coupling of different modes. The information on natural characteristic modes and modal weighting coefficient helped identify the modal fields that may potentially participate in the beamforming of the antenna array. By investigating their respective radiation patterns, the potential coupling of modes was analyzed for beamforming in theta and phi directions. Furthermore, CMA offers valuable guidelines on selectively exciting the desired modes. Three cases have been discussed by selecting the different phase combinations of feeding ports to describe the potential of multi-dimensional coverage of a multibeam array. The measured results of the fabricated prototype showed that the proposed dual-beam antenna array is physically realizable. The paper also discussed the limitations of the antenna array and the potential areas to optimize the structure. The proposed design is a good candidate for future applications where multiple beams can be scanned from a simple, low-cost structure in theta and phi directions.

ACKNOWLEDGMENT

IEEE OJAP encourages responsible authorship practices and the provision of information about the specific contribution of each author.

REFERENCES

[1] H. Nawaz and I. Tekin, "Ten switched beams with 2 × 2 series-fed 2.4 GHzarray antenna and a simple beam-switching network." *Int J RF Microw Comput Aided Eng.*, vol. 30, Feb. 2020, Art. no. e22184, [Online]. Available: https://doi.org/10.1002/mmce.22184

[2] M. Khalily, R. Tafazolli, T. A. Rahman, and M. R. Kamarudin, "Design of phased arrays of series-fed patch antennas with reduced number of the controllers for 28-GHz mm-Wave applications," *IEEE Antennas Wireless Propag. Lett.*, vol. 15, pp. 1305–1308, 2016, doi: 10.1109/LAWP.2015.2505781.

[3] A. Elsherbini, J. Wu, and K. Sarabandi, "Dual polarized wideband directional coupled sectorial loop antennas for radar and mobile base-station applications," *IEEE Trans. Antennas Propag.*, vol. 63, no. 4, pp. 1505–1513, Apr. 2015.

[4] K. N. Khac et al., "A design of circularly polarized array antenna for X-band cubesat satellite communication," in *Proc. Int. Conf. Adv. Technol. Commun. (ATC)*, Ho Chi Minh City, Vietnam, 2018, pp. 53–56, doi: 10.1109/ATC.2018.8587574.

[5] X. Fu, Z. Zhang, and J. Wang, "A compact frequency scanning planar array using characteristic mode analysis," *IEEE Antennas Wireless Propag. Lett.*, vol. 20, no. 9, pp. 1666–1670, Sep. 2021, doi: 10.1109/LAWP.2021.3092366.

[6] C. J. You et al., "Frequency-and pattern-reconfigurable antenna array with broadband tuning and wide scanning angles," *IEEE Trans. Antennas Propag.*, vol. 71, no. 6, pp. 5398–5403, Jun. 2023, doi: 10.1109/TAP.2023.3255647.

[7] F. A. Dicandia, S. Genovesi, and A. Monorchio, "Advantageous exploitation of characteristic modes analysis for the design of 3-D null-scanning antennas," *IEEE Trans. Antennas Propag.*, vol. 65, no. 8, pp. 3924–3934, Aug. 2017, doi: 10.1109/TAP.2017.2716402.

[8] F. A. Dicandia, S. Genovesi, and A. Monorchio, "Null-steering antenna design using phase-shifted characteristic modes," *IEEE Trans. Antennas Propag.*, vol. 64, no. 7, pp. 2698–2706, Jul. 2016, doi: 10.1109/TAP.2016.2556700.

[9] S. Radavaram and M. Pour, "Wideband radiation reconfigurable microstrip patch antenna loaded with two inverted U-slots," *IEEE Trans. Antennas Propag.*, vol. 67, no. 3, pp. 1501–1508, Mar. 2019, doi: 10.1109/TAP.2018.2885433.

[10] N. Lusdyk and M. Khan, "On the use of characteristic mode analysis for dual beam antenna array," in *Proc. 17th Eur. Conf. Antennas Propag. (EuCAP)*, Florence, Italy, 2023, pp. 1–4, doi: 10.23919/EuCAP57121.2023.10133179.

[11] D. Manteuffel, F. H. Lin, T. Li, N. Peitzmeier, and Z. N. Chen, "Characteristic mode-inspired advanced multiple antennas: Intuitive insight into element-, interelement-, and array levels of compact large arrays and metantennas," *IEEE Antennas Propag. Mag.*, vol. 64, no. 2, pp. 49–57, Apr. 2022, doi: 10.1109/MAP.2022.3145714.

[12] L. Mörlein and D. Manteuffel, "Understanding single-element beamforming using characteristic modes and a change of basis," in *Proc. 16th Eur. Conf. Antennas Propag. (EuCAP)*, Madrid, Spain, 2022, pp. 1–3, doi: 10.23919/EuCAP53622.2022.9769639.

[13] M. Khan and M. Chowdhury, "Analysis of modal excitation in wideband slot-loaded microstrip patch antenna using theory of characteristic modes," *IEEE Trans. Antennas Propag.*, vol. 68, no. 11, pp. 7618–7623, Nov. 2020, doi: 10.1109/TAP.2020.2989867.

[14] M. Khan and D. Chatterjee, "Analysis of reactive loading in a U-slot microstrip patch using the theory of characteristic modes [Antenna Applications Corner]," *IEEE Antennas Propag. Mag.*, vol. 60, no. 6, pp. 88–97, Dec. 2018, doi: 10.1109/MAP.2018.2870653.

[15] Y. Liu, A. Ren, H. Liu, H. Wang, and C.-Y.-D. Sim, "Eight-port MIMO array using characteristic mode theory for 5G smartphone applications," *IEEE Access*, vol. 7, pp. 45679–45692, 2019, doi: 10.1109/ACCESS.2019.2909070.

[16] G. Cheng, M. Tian, L. Zhang, and Z. Huang, "Design of dual-port pattern-reconfigurable MIMO antenna with four operating states using the TCM," *IEEE Antennas Wireless Propag. Lett.*, vol. 22, no. 1, pp. 169–173, Jan. 2023, doi: 10.1109/LAWP.2022.3206324.
[17] Y. Qin, L. Zhang, C. Mao, and H. Zhu, "Low-profile compact tri-band multimode reconfigurable antenna using characteristic mode analysis," *IEEE Trans. Antennas Propag.*, vol. 71, no. 7, pp. 6144–6149, Jul. 2023, doi: 10.1109/TAP.2023.3266055.
[18] Z. Zhang, S. Cao, and J. Wang, "Azimuth-pattern reconfigurable planar antenna design using characteristic mode analysis," *IEEE Access*, vol. 9, pp. 60043–60051, 2021, doi: 10.1109/ACCESS.2021.3073706.
[19] H. Jaafar, S. Collardey, and A. Sharaiha, "Characteristic modes approach to design compact superdirective array with enhanced bandwidth," *IEEE Trans. Antennas Propag.*, vol. 66, no. 12, pp. 6986–6996, Dec. 2018, doi: 10.1109/TAP.2018.2874691.
[20] Z. Zhang, X. Fu, and S. Cao, "Design of a vertically polarized patch antenna with switchable near-endfire beam using characteristic mode analysis," *IEEE Antennas Wireless Propag. Lett.*, vol. 19, no. 7, pp. 1157–1161, Jul. 2020, doi: 10.1109/LAWP.2020.2992486.
[21] T. Li and Z. N. Chen, "Design of dual-band metasurface antenna array using Characteristic Mode Analysis (CMA) for 5G millimeter-wave applications," in *Proc. IEEE-APS Topical Conf. Antennas Propag. Wireless Commun. (APWC)*, Cartagena, Colombia, 2018, pp. 721–724, doi: 10.1109/APWC.2018.8503769.
[22] Y. Chen and C.-F. Wang, "Reactively loaded antenna array design with characteristic modes and DE algorithm," in *Proc. IEEE Int. Sym. Antennas Propag.*, Chicago, IL, USA, 2012, pp. 1–2, doi: 10.1109/APS.2012.6348999.
[23] F. A. Dicandia, S. Genovesi, and A. Monorchio, "Efficient excitation of characteristic modes for radiation pattern control by using a novel balanced inductive coupling element," *IEEE Trans. Antennas Propag.*, vol. 66, no. 3, pp. 1102–1113, Mar. 2018, doi: 10.1109/TAP.2018.2790046.
[24] A. Adam Salih, Z. N. Chen, and K. Mouthaan, "Characteristic mode analysis and metasurface-based suppression of higher order modes of a 2×2 closely spaced phased array," *IEEE Trans. Antennas Propag.*, vol. 65, no. 3, pp. 1141–1150, Mar. 2017, doi: 10.1109/TAP.2016.2647683.
[25] H. Li, Y. Chen, and U. Jakobus, "Synthesis, control, and excitation of characteristic modes for platform-integrated antenna designs: A design philosophy," *IEEE Antennas Propag. Mag.*, vol. 64, no. 2, pp. 41–48, Apr. 2022, doi: 10.1109/MAP.2022.3145722.
[26] H. Li, S. Sun, W. Li, M. Wu, and C. Zhou, "Systematic pattern synthesis for single antennas using characteristic mode analysis," *IEEE Trans. Antennas Propag.*, vol. 68, no. 7, pp. 5199–5208, Jul. 2020, doi: 10.1109/TAP.2020.2978939.
[27] Z. Liang, J. Ouyang, F. Yang, and L. Zhou, "Design of license plate RFID tag antenna using characteristic mode pattern synthesis," *IEEE Trans. Antennas Propag.*, vol. 65, no. 10, pp. 4964–4970, Oct. 2017, doi: 10.1109/TAP.2017.2734071.
[28] N. Peitzmeier and D. Manteuffel, "Beamforming concept for multi-beam antennas based on characteristic modes," in *Proc. IEEE Int. Symp. Antennas Propag. USNC/URSI Nat. Radio Sci. Meet.*, Boston, MA, USA, 2018, pp. 1113–1114, doi: 10.1109/APUSNCURSINRSM.2018.8609434.
[29] Y. Hu, X. Zhang, and T. Chi, "A 28-GHz hybrid beamforming transmitter with spatial notch steering enabling concurrent dual data streams for 5G MIMO applications," *IEEE J. Solid-State Circuits*, early access, May 17, 2024, doi: 10.1109/JSSC.2024.3399220.
[30] X. Cheng, X. Yuan, W. Jiang, L. Zhu, Y. Zuo, and Y. Zhang, "Deep active learning for mmWave array-based multi-source AoA tracking," *IEEE Trans. Wireless Commun.*, early access, May 3, 2024, doi: 10.1109/TWC.2024.3391850.

MAHRUKH KHAN (Member, IEEE) is an Assistant Professor with The College of New Jersey (TCNJ), NJ, USA. She is also a Co-Director of Microwave and Wireless Communication Lab, TCNJ. She has published more than 30 articles and conference papers in renowned journals and peer-reviewed conferences in her field of research. Her research articles and conference papers have received over 350+ citations in a short period. She was selected as a 2022 IEEE Antennas and Propagation Young Professional Ambassador. She also won a TCNJ Early Career Faculty Excellence Award from the TCNJ Faculty Senate in 2024. She has won an Honorable Mention in the International 2015 Altair FEKO student competition. She has won the prestigious UMKC School of Graduate Studies Fellowship for outstanding research. She has served as a Reviewer of top-notch peer-reviewed journals such as IEEE ANTENNAS AND PROPAGATION MAGAZINE and *IET Microwaves, Antennas, and Propagation*. She is a Senior Member of URSI and an Active Member of IEEE Young Professionals and IEEE Women in Engineering Societies.

TALHA MURAD (Student Member, IEEE) is currently pursuing the B.Sc. degree in electrical engineering with The College of New Jersey. His specializing in microstrip antenna design for IoT and 5G applications. He is a Vice President of the IEEE Student Chapter and an Executive Board Member of HKN, he actively engages in leadership and collaborative initiatives within the engineering community. With aspirations to lead in the telecommunications field, his aims to contribute significantly to the advancements of modern communication systems, particularly in the realms of 5G and IoT. His research focuses on developing innovative solutions to enhance wireless communication technologies.

NICHOLAS LUSDYK received the B.Sc. degree in electrical engineering from The College of New Jersey in 2022. During this time, he worked with Microwave and Communication Lab on antenna arrays for 5G communications. He is working as a Research and Development Engineer with Amplifier Research Corporation, NJ, USA.